

Precipitation Behavior and Strengthening Effect of (Ti,Mo)C Particles in a Martensitic Steel

Jin Xiaokun^{1,2}, Xu Le¹, Yu Wenchao¹, Yao Kefu², Shi Jie¹, Wang Maoqiu¹

¹ Central Iron and Steel Research Institute (CISRI), Beijing 100081, China; ² Tsinghua University, Beijing 100084, China

Abstract: To study the precipitation behavior and strengthening effect of (Ti,Mo)C particles, Cr-Mo steel with added Ti was austenitized at 880 and 1350 °C followed by oil quenching and tempering. The chemical extraction phase analysis results show that some (Ti,Mo)C particles were found to have size distributions within the range of 18~36 nm, 36~60 nm, and 60~96 nm when the steel was austenitized at 880 °C and particles were precipitated during hot rolling. When the austenitized temperature was 1350 °C, some new (Ti,Mo)C particles appeared with sizes ranging within 1~5 nm, precipitated during tempering. These (Ti,Mo)C particles demonstrated a distinct secondary hardening platform with a strengthening increment of approximately 165 MPa. The atomic ratio of Ti/Mo in the (Ti,Mo)C particles precipitated during tempering decreased to approximately 1 as the tempering temperature increased.

Key words: martensitic steel; tempering; (Ti,Mo)C precipitates; strengthening

Medium-carbon Cr-Mo martensitic steels have been widely used in high-strength bolts due to their combination of high strength and good ductility after quenching and tempering^[1]. To prevent hydrogen embrittlement of high-strength bolts, other elements including Nb, V, and Ti can be added to the Cr-Mo martensitic steels to form carbides that can act as hydrogen trap sites^[2]. These elements can also contribute to a secondary hardening effect, leading to high strength after high-temperature tempering. Among these elements, Ti is unique because it can form (Ti,Mo)C particles when combined with Mo; however, research has not yet clarified the precipitation behavior and strengthening effect of (Ti,Mo)C particles.

Some studies have investigated the precipitation behavior of (Ti,Mo)C particles in HSLA steels during hot rolling, which indicate different strengthening effects. Funakawa et al.^[3] reported that the precipitation strengthening of interphase-precipitated (Ti,Mo)C particles was approximately 300 MPa. Yen^[4] and Wang^[5] each reported that the yield strength could be increased by 400 MPa through

interphase-precipitated (Ti,Mo)C particles. Kim et al.^[6] found that the contribution to yield strength from the precipitation strengthening of (Ti,Mo)C particles was in the range of 154~320 MPa depending on rolling conditions. Sun^[7] reported that the precipitation-strengthening effect from (Ti,Mo)C particles was as low as 110 MPa; however, the precipitation behavior of (Ti,Mo)C particles during tempering and the associated strengthening effect have rarely been investigated. This research aims to examine these phenomena using a medium-carbon Cr-Mo steel with added Ti.

1 Experiment

The chemical composition of the experimental steel is listed in Table 1. Hot-rolled wire rods with a diameter of 12 mm were used in this study. The experimental steel was first austenitized at either 880 °C or 1350 °C for 5 min before being oil quenched to room temperature, tempered at 400~700 °C for 2 h, and finally air-cooled to room temperature. The sample was signified by austenitizing and tempering temperatures such as 880-500 for the 880 °C

Received date: January 15, 2019

Foundation item: National Key Research and Development Program (2016YFB0300104, 2016YFB0300102, 2017YFB0304802)

Corresponding author: Jin Xiaokun, Candidate for Ph. D., Institute for Special Steels, Central Iron and Steel Research Institute (CISRI), Beijing 100081, P. R. China, E-mail: 2545835925@qq.com

Copyright © 2020, Northwest Institute for Nonferrous Metal Research. Published by Science Press. All rights reserved.

austenitizing and 500 °C tempering sample. Hardness was determined by a VH-5 Vickers hardness tester with a 5 kg load according to Chinese national standard GB/T 4310.1-2012, and the average value of Vickers hardness was calculated from five readings. Tensile samples ($\Phi 5$ mm, parallel length of 30 mm) were tested at room temperature using a WE-300 machine according to Chinese national standard GB/T 228.1-2010, and three specimens were tested to record the mean values. The structures, number, and chemical compositions of precipitates were quantitatively analyzed by chemical extraction phase analysis. Precipitates were electrolytically extracted using 10 g/L tetramethyl ammonium chloride + 10% acetylacetone methanol ($i = 0.03\sim 0.05$ A/cm², $T = -5\sim 0$ °C). After collecting, cleaning, and drying, a PANalytical X'Pert MPD X-ray diffractometer (Cu K α at 40 kV and 40 mA) was used to determine the structure of the precipitates. The contents of the elements in the precipitates were measured using inductively coupled plasma-mass spectrometry (ICP-AES). The M_3C particles were dissolved, and MC particles were retained using a 5%~10% (V/V) hydrochloric acid ethyl alcohol solution. Then, size distributions of the MC phase were determined with a powder X-ray diffractometer (PANalytical X'Pert MPD)/Kratky small-angle scattering goniometer with Cu K α at 40 kV and 40 mA according to ISO/TS13762 and GB/T 13221 standards. The dislocation density was measured by a BRUKER D8 X-ray diffractometer with Co K α at 40 kV and 35 mA. Scanning electron microscopy (SEM, HITACHI S-4300) and high-resolution field-emission transmission electron

microscopy (TEM, JEM-2100F) were used to observe the microstructure and precipitates. Carbon extraction replicas were used for HRTEM observation, prepared by plating a carbon film of 20~30 nm thickness on the sample surface etched with 4% nital after being mechanically polished. Then, the carbon films were extracted with 4% nital and taken out with a copper net.

2 Results and Discussion

2.1 SEM observation of microstructure

Fig. 1 shows SEM micrographs of the samples after being austenitized at 880 °C and tempered at different temperatures. The as-quenched sample exhibited a typical martensitic microstructure, and it was transformed to tempered martensite as the tempering temperature increased.

Tempered martensite lath structures were essentially intact in the temperature range of 400~500 °C and gradually changed within the temperature range of 550~600 °C. The lath structures disappeared completely in the temperature range of 650~700 °C.

Fig.2 shows SEM micrographs of samples austenitized at 1350 °C and tempered at different temperatures; the microstructure was clearly coarser than in the 880 °C austenitized samples. The as-quenched sample also showed a typical martensitic microstructure and was transformed to tempered martensite as the tempering temperature rose. The tempered martensite lath structures were effectively intact in the range of 400~550 °C, and only a small number of them changed within 600~650 °C. The lath structures disappeared completely by 700 °C, indicating a delayed change in the lath structure.

Table 1 Chemical composition of experimental steel (wt%)

C	Si	Mn	S	P	Cr	Mo	Ti	N
0.30	0.15	0.31	0.002	0.006	1.36	0.18	0.08	0.0049

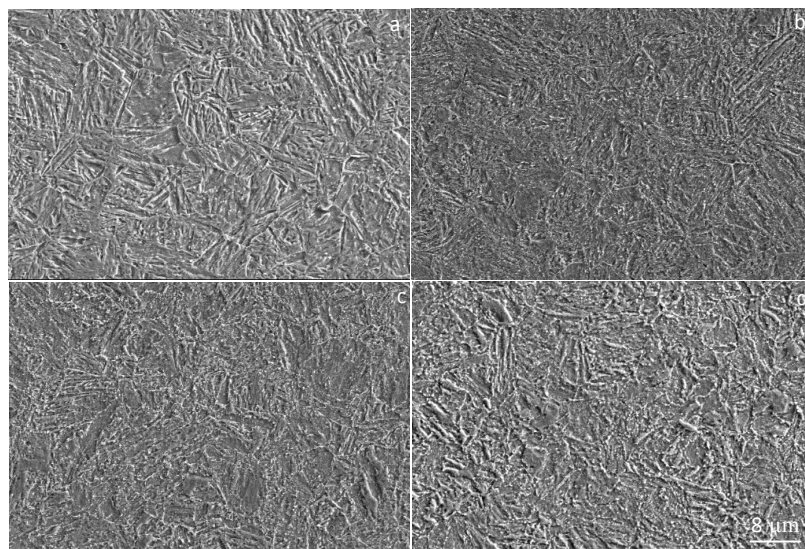


Fig.1 SEM images of different heat-treated samples: (a) 880-Q; (b) 880-450; (c) 880-550; (d) 880-650

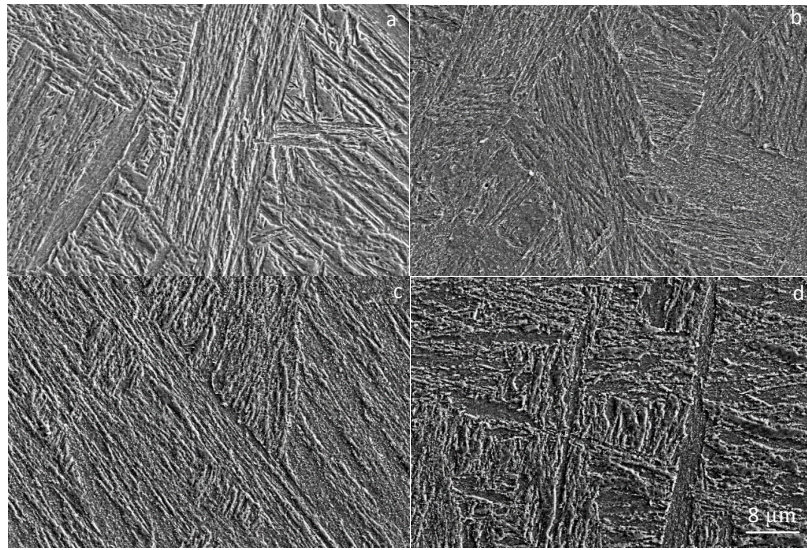


Fig.2 SEM images of different heat-treated samples: (a) 1350-Q, (b) 1350-450, (c) 1350-550, and (d) 1350-650

2.2 Chemical extraction phase analysis and TEM observation of precipitates

The precipitates in the as-received hot-rolled wire rod were mainly M_3C with a mass percent as high as 3.8%, as shown in Table 2. Some $M(C,N)$ precipitates were also identified in the rod, demonstrating a content of 0.13% consisting mainly of Ti and Mo alloy elements, as shown in Table 3. These carbides are signified as (Ti,Mo)C in this research although they exhibited a chemical form of $(Ti_{0.853}Mo_{0.147})(C_{0.824}N_{0.176})$.

When the samples were austenitized at 880 °C and oil quenched, many of the M_3C precipitates dissolved into austenite. The measured M_3C content was reduced from 3.8% to 1.276%, as shown for 880-Q in Table 4, indicating that most carbon were remained in the solid solution after quenching.

However, the amount of the (Ti,Mo)C precipitates did not change evidently, as indicated for 880-Q in Table 5, suggesting that this type of precipitate was highly stable at an austenitizing temperature of 880 °C. After tempering in the

temperature range of 400~700 °C, the fraction of M_3C gradually increased in line with tempering temperature (Table 4), whereas the fraction of (Ti,Mo)C precipitates remained unchanged at 0.12 wt% (Table 5). The Ti and Mo contents in the MC phase were also unchanged, similar to the hot-rolling state. The small-angle scattering results illustrated that the size distributions of these samples were primarily within 18~36 nm, 36~60 nm, and 60~96 nm. The result of the hot-rolled sample is presented in Fig.3.

As shown in Tables 6 and 7, the types of precipitates in specimens austenitized at 1350 °C and tempered at different temperatures were mainly M_3C and MC. Like those quenched at 880 °C, M_3C mainly contained Fe, Mn, Cr, Mo, and C elements. MC included mostly Ti, Mo, and C elements. The fraction of cementite also increased gradually with an increase in tempering temperature.

In contrast to quenching at 880 °C, the fraction of the MC phase in the as-quenched sample was relatively low but began to increase substantially when tempered at 550 °C. The precipitation amount increased gradually as the tempering

Table 2 Elements in M_3C in as-received hot-rolled wire rod samples (wt%)

Sample	Fe	Mn	Cr	Mo	C	Total
Hot-Rolled	3.162	0.046	0.308	0.031	0.255	3.802

Table 3 Elements in $M(C,N)$ in as-received hot-rolled wire rod samples (wt%)

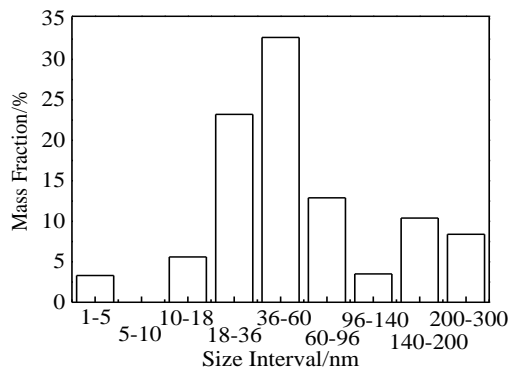
Sample	Ti	Mo	N	C	Total
Hot-Rolled	0.078	0.027	0.0047	0.019	0.129

Table 4 Elements in M_3C in samples austenitized at 880 °C and tempered at different temperatures (wt%)

Sample	Fe	Mn	Cr	Mo	C	Total
880-Q	1.114	0.005	0.058	0.014	0.085	1.276
880-400	2.435	0.010	0.058	0.010	0.180	2.693
880-450	2.669	0.014	0.084	0.010	0.199	2.976
880-500	3.118	0.033	0.180	0.019	0.240	3.590
880-550	3.220	0.059	0.327	0.035	0.262	3.903
880-600	3.155	0.072	0.444	0.028	0.267	3.966
880-650	2.757	0.077	0.569	0.029	0.248	3.680
880-700	3.217	0.083	0.774	0.031	0.297	4.402

Table 5 Elements in $M(C,N)$ in samples austenitized at 880 °C and tempered at different temperatures (wt%)

Sample	Ti	Mo	N	C	Total
880-Q	0.076	0.024	0.0049	0.018	0.123
880-400	0.074	0.024	0.0048	0.017	0.120
880-450	0.074	0.024	0.0048	0.017	0.120
880-500	0.076	0.027	0.0047	0.018	0.126
880-550	0.076	0.026	0.0048	0.018	0.125
880-600	0.073	0.032	0.0047	0.018	0.128
880-650	0.075	0.030	0.0048	0.018	0.128
880-700	0.080	0.037	0.0049	0.020	0.142

**Fig.3** Size distributions of (Ti,Mo)C particles in as-received hot-rolled wire rod samples

temperature grew. Although the tempering temperature reached as high as 700 °C, the titanium did not precipitate completely. The Ti and Mo contents in the MC phase also increased, especially the latter.

Small-angle scattering results indicate that the size distributions in these samples were mainly within 1~5 nm, as shown in Fig. 4a. When the tempering temperature was 650 °C and 700 °C, some precipitates grew to 5~10 nm and 10~18 nm, respectively. A large portion of precipitates were within 200~300 nm, presenting as undissolved TiN and Ti_2CS as displayed in Fig.4b.

The HRTEM morphology, selected area electron diffraction (SAED) pattern, and energy dispersive spectrometer (EDS)

Table 6 Elements in M_3C in samples austenitized at 1350 °C and tempered at different temperatures (wt%)

Sample	Fe	Mn	Cr	Mo	C	Total
1350-Q	1.368	0.004	0.027	0.013	0.101	1.513
1350-400	2.506	0.008	0.046	0.012	0.184	2.756
1350-450	2.731	0.010	0.057	0.013	0.201	3.012
1350-500	2.882	0.020	0.097	0.020	0.216	3.235
1350-550	2.945	0.040	0.210	0.039	0.232	3.466
1350-600	3.043	0.066	0.354	0.038	0.252	3.753
1350-650	2.970	0.078	0.602	0.037	0.266	3.953
1350-700	2.731	0.075	0.669	0.035	0.254	3.764

Table 7 Elements in M(C,N) in samples austenitized at 1350 °C and tempered at different temperatures (wt%)

Sample	Ti	Mo	N	C	Total
1350-Q	0.034	0.003	0.0045	0.005	0.047
1350-400	0.034	0.003	0.0044	0.005	0.047
1350-450	0.033	0.003	0.0044	0.005	0.046
1350-500	0.037	0.005	0.0046	0.006	0.053
1350-550	0.055	0.024	0.0047	0.013	0.097
1350-600	0.059	0.040	0.0048	0.016	0.120
1350-650	0.069	0.056	0.0049	0.020	0.150
1350-700	0.073	0.065	0.0049	0.022	0.165

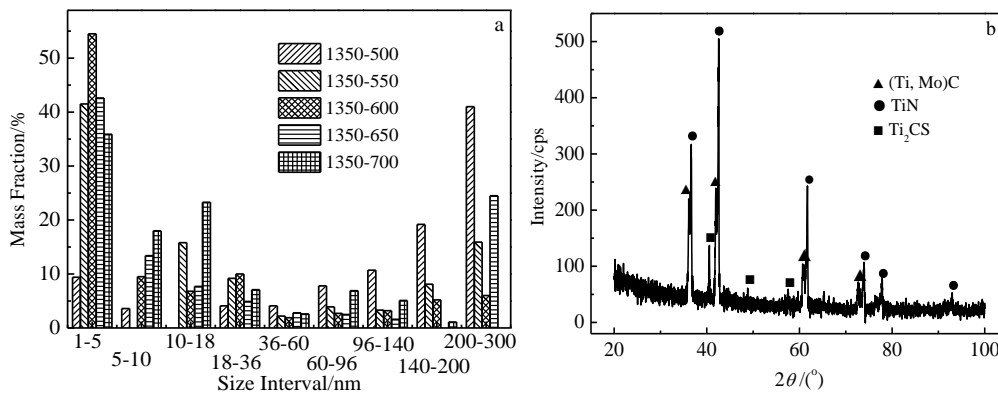


Fig.4 Size distributions (a) and XRD pattern (b) of extraction particles in 1350-500, 1350-550, 1350-600, 1350-650, and 1350-700 samples

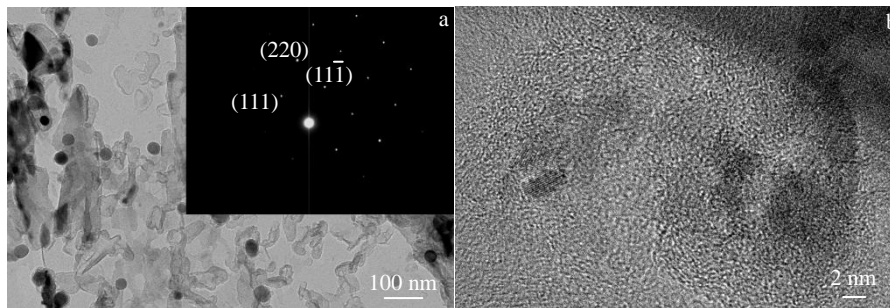


Fig.5 HRTEM images of (Ti,Mo)C precipitates: (a) 30CrMoTi, 880-450 and (b) 30CrMoTi, 1350-700

results substantiated the presence of (Ti,Mo)C precipitates in the tempered samples, as shown in Fig.5 for the 880-450 and 1350-700 samples.

These results were consistent with those of the chemical extraction phase analysis.

2.3 Mechanical properties

The mechanical properties of samples austenitized at 880 °C and tempered at different temperatures are shown in Fig.6. The Vickers hardness, tensile strength, and yield strength declined linearly with the increasing tempering temperature.

The mechanical properties of samples austenitized at 1350 °C and tempered at different temperatures are shown in Fig.7. The Vickers hardness, tensile strength, and yield

strength fell linearly as the tempering temperature increased up to 500 °C. In the temperature range of 550-650 °C, the hardness and strength did not decline clearly, implying a secondary hardening platform.

2.4 Precipitation behavior

Table 3 reveals that nearly all titanium in steel was precipitated during the hot-rolling process. According to the solid solubility product formula^[8],

$$\log_{10}[\text{Ti}][\text{C}] = -\frac{7000}{T} + 2.75 \quad (1)$$

little (Ti,Mo)C was dissolved during the austenitizing process at 880 °C; therefore, no sufficient Ti element was precipitated during the tempering process. Fig.3 indicates that the size distributions of (Ti,Mo)C particles in the

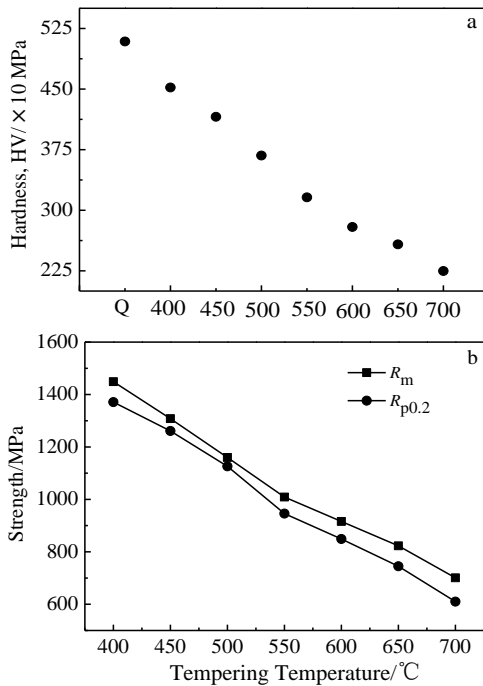


Fig.6 Vickers hardness (a) and strength (b) of samples quenched at 880 °C and tempered at different temperatures

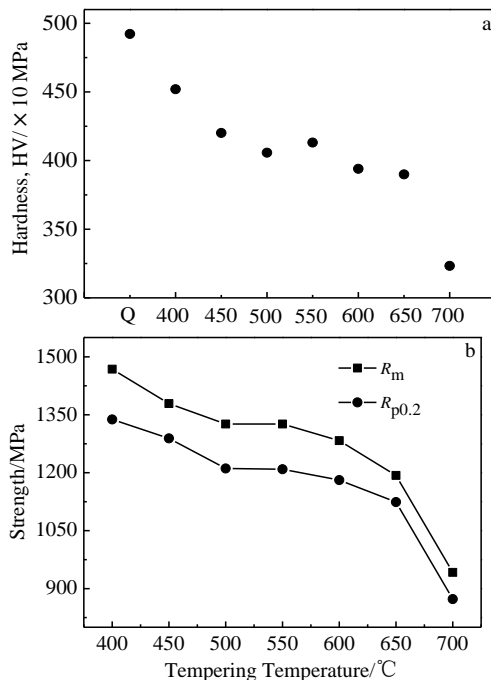


Fig.7 Vickers hardness (a) and strength (b) of samples quenched at 1350 °C and tempered at different temperatures

as-received hot-rolled wire rod were primarily within 36~60 nm. The HRTEM images of (Ti,Mo)C particles in the 880-450 samples also reveal sizes within this range. Peng et al.^[9] reported that strain-induced TiC carbides formed in the hot-rolling process were in the range of 10~40 nm. Wang et

al.^[10] found that the (Ti,Mo)C carbides precipitated in austenite were in the range of 20~40 nm. This finding suggests that these observed (Ti,Mo)C particles all formed during hot rolling and were retained in the subsequent quenching and tempering process. Thus, no (Ti,Mo)C particles appeared to be precipitated during the tempering process after being quenched at 880 °C. The chemical composition of (Ti,Mo)C precipitates did not change much, as shown in Table 5 and Fig.8, and the atomic ratio of Ti/Mo in (Ti,Mo)C precipitates was within the range of 5~4. In the calculation, N was expected to be consumed by forming TiN.

According to Eq.(1), nearly all (Ti,Mo)C particles precipitated in the hot-rolling process could be dissolved in austenite at 1350 °C. The phase analysis results shown in Table 7 reveal that nearly all the titanium dissolved in austenite apart from TiN. No (Ti,Mo)C particles were newly precipitated at the tempering temperatures of 400~500 °C. A large number of (Ti,Mo)C particles began to precipitate at 550 °C, and a small secondary hardening peak appeared at this temperature. Wei^[11] found that 0.42C-0.30Ti steel also exhibited a secondary hardening peak at 550 °C when quenched at 1350 °C. K. E.-Fawakhry^[12] reported that added titanium can increase the tempering resistance in the early stages of tempering and cause secondary hardening at 550~600 °C. In this work, the secondary hardening temperature reached a temperature of 650 °C. As Mo reduced the growth and coarsening rate of nano-sized carbides, the growth rate of (Ti,Mo)C in Ti-Mo steel was less than that of TiC in Ti steel^[13]. As displayed in Fig. 4, the size of the (Ti,Mo)C particles was mainly within 1~5 nm; only a few (Ti,Mo)C particles measured to be 1~5 nm later expanded to 5~10 and 10~18 nm at 650 °C, and a large number of 1~5 nm (Ti,Mo)C particles still existed at 700 °C. Therefore, the (Ti,Mo)C particles could produce secondary hardening at a higher temperature than TiC particles, as shown in Fig. 7.

N was expected to be consumed by forming TiN. The atomic ratio of Ti/Mo in the residual (Ti,Mo)C precipitates after being quenched and tempered at 400/450 °C was approximately 12 as see in Fig.9, identical to that of the as-quenched sample and much higher than that of 5~4 in the hot-rolled sample. This difference was presumably due to a greater amount of Mo in the (Ti,Mo)C particles having dissolved into the austenite during austenitizing at 1350 °C. After tempering, the Mo elements began to diffuse into (Ti,Mo)C particles at 500 °C, and the atomic ratio of Ti/Mo decreased sharply at this temperature. With an increase in the tempering temperature, the atomic ratio of Ti/Mo declined further before finally stabilizing at approximately 1 when tempered at 600~700 °C.

Cheng et al.^[14] reported that the atomic ratio of Ti/Mo in the (Ti,Mo)C increased in line with the precipitate size in the low-carbon, low-alloy hot-rolled sheet. When the precipitate size grew from 5 nm to 10 nm, the atomic ratio of Ti/Mo in

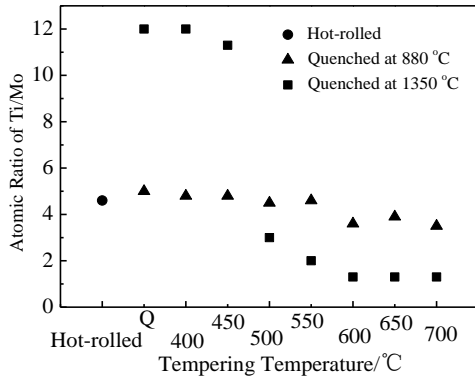


Fig.8 Atomic ratio of Ti/Mo in (Ti,Mo)C precipitates

the precipitated phase increased from 0.53 to 1.65. The author stated that, when the precipitation phase was sufficiently small, the nucleation process of (Ti,Mo)C was dominated by the interface energy, and the Mo-rich (Ti,Mo)C phase was more advantageous to reduce the interface energy. Thus, a coherent interface could be more easily formed with the matrix. When the precipitation phase expanded to a certain size, the Gibbs free energy of the system began to play a leading role. More Ti atoms were gathered at the core to reduce the Gibbs free energy of the system and increase the Ti/Mo atomic ratio. First-principles calculations^[15] indicate that the replacement of Ti by Mo in the TiC lattice is energetically unfavorable with respect to the formation energy; however, it decreases the misfit strain between the carbide and ferrite matrix, which is critically important during the early stages of precipitation, thus favoring the substitution of Ti by Mo. Wang et al.^[16] found that the atomic ratio of Ti/Mo in the (Ti,Mo)C increased with an isothermal holding time at 925 °C or with particle growth when studying the carbide precipitation behavior in austenite in 0.04%C-0.10%Ti-0.21%Mo low-carbon steel. Simultaneously, the calculated results conducted by the author using Thermo-Calc with the TCFE6 database showed that the equilibrium chemical composition of the MC phase approached the pure TiC at temperatures above 800 °C. As the temperature declined, the equilibrium atomic fraction of Mo in the MC phase increased. When the temperature fell to below 700 °C, the increase in the atomic fraction of Mo with temperature accelerated, and the atomic ratio of Mo/Ti was approximately 1.0 in the temperature range of 500~600 °C. Nagao et al.^[17] reported that (Ti,Mo)C precipitates were presumably formed during hot rolling (strain-induced precipitation) and tempering. Quantification of the EDX results and an extracted residue analysis revealed an atomic ratio of Ti/Mo for these nano-sized carbide precipitates of ~1:1. As shown in Fig.4, the newly precipitated (Ti,Mo)C particles in this study with size mostly measured within 1~5 nm, presumably because they were still in the early stages of precipitation. The nucleation process of (Ti,Mo)C was dominated by interface energy, and the replacement of Ti by

Mo in the TiC lattice was beneficial for reducing the misfit strain between the carbide and ferrite matrix along with the interface energy; therefore, the atomic ratio of Ti/Mo was lower. When the tempering temperature rose to 600~700 °C, the atomic ratio of Ti/Mo in the (Ti,Mo)C particle approached ~1:1, identical to the calculation result found by Wang et al.^[16] and Nagao et al.^[17]

2.5 Precipitation strengthening effect

The Vickers hardness, tensile strength, and yield strength of samples austenitized at 880 °C and tempered at different temperatures decreased linearly as the tempering temperature increased, as shown in Fig.6. These findings were consistent with the results of an experiment on AISI 4340 steel reported by Lee^[18]. The strengthening mechanisms of steels mainly include solid solution strengthening, grain refinement strengthening, precipitation strengthening, and dislocation strengthening. No new (Ti, Mo)C particles formed during the tempering process after being quenched at 880 °C, and the grain size did not change during the tempering process. The solid solution strengthening of samples tempered at different temperatures after being quenched at 880 °C were calculated based on the chemical-extraction-phase analysis results and the solid solution strengthening empirical formula^[19]:

$$\sigma_s = 4570[C] + 4570[N] + 470[P] + 83[Si] + 37[Mn] + 11[Mo] + 80[Ti] - 30[Cr] \quad (2)$$

where [X] represents the mass fraction of the element X. The solid solution strengthening value and measured yield strength of 880-400 were taken as the reference values. Reduced solid solution strengthening was equal to the solid solution strengthening value of 880-400 minus the other solid solution strengthening values, and the reduced yield strength was obtained in the same way; calculation results are listed in Table 8.

Table 8 shows that the reduction in solid solution strengthening was exactly equal to the measured yield strength reduction at tempering temperatures within the range of 400~500 °C; that is, solid solution strengthening reduction was responsible for reduced yield strength within the tempering temperature range of 400~500 °C, and the dislocation strengthening can be ignored. This finding may be attributed to the fact that the tempered martensite lath remained in this temperature range, as shown in Fig.1. Tempered martensite lath was decomposed or even disappeared at tempering temperatures of 550~700 °C, and the dislocation strengthening could not be ignored. Solid solution strengthening and dislocation density decreased over the course of tempering and were primarily accountable for decreases in hardness and strength^[20], as indicated by the calculation results in Table 8.

Table 8 shows that when the tempered martensite lath remained (tempered at 400~500 °C), the reduction in solid solution strengthening was exactly equal to the measured yield strength reduction. The dislocation strengthening could be ignored. As for samples quenched at 1350 °C, the

Table 8 Reduced solid solution strengthening and reduced measured yield strength after quenched at 880 °C and tempered at different temperatures (MPa)

Sample	Solid solution strengthening	Reduced solid solution strengthening	Reduced measured yield strength
880-400	457	—	—
880-450	371	86	110
880-500	181	276	245
880-550	84	374	425
880-600	64	393	522
880-650	155	303	626
880-700	5	453	761

nano-sized (Ti,Mo)C particles largely precipitated after 500 °C tempering; the (Ti,Mo)C particles size distributions are presented in Fig. 4. The average particle diameter of (Ti,Mo)C particles measured to be 1~5 nm, 5~10 nm, 10~18 nm, and 18~36 nm was 3, 8, 14, and 27 nm, respectively. When the average particle diameter exceeded 40 nm, the precipitation contribution was not significant. The effect of precipitation strengthening can be described by Eq. (3)^[9],

$$\sigma_p = \frac{5.9f^{1/2}}{\bar{X}} \ln\left(\frac{\bar{X}}{2.5 \times 10^{-4}}\right) \quad (3)$$

where \bar{X} is the average diameter of precipitates in μm ; and f is the volume fraction of precipitates, calculated as follows:

$$f = (M - [M]) \cdot \frac{A_M + xA_X}{A_M} \cdot \frac{d_{\text{Fe}}}{100d_{\text{MX}_x}} \quad (4)$$

where $(M - [M])$ is the total amount of M elements (Ti and Mo were each taken into account) that have precipitated, and d_{Fe} , d_{MX_x} denote the density of the iron matrix (7.85 g/cm^3) and precipitate phase (4.94 g/cm^3 for TiC), respectively, A_M and A_X are the atomic weights of elements M (Ti: 47.867) and X (C: 12.01), respectively. The precipitation strengthening of different particle sizes was calculated, and the total amount of precipitation strengthening was superimposed on the root mean square^[19], calculation results are shown in Table 9.

Table 9 Precipitation strengthening of different particle sizes and total amount of precipitation strengthening in different heat-treated samples

Sample	1~5 nm	5~10 nm	10~18 nm	18~36 nm	Total amount
1350-450	—	—	—	—	—
1350-500	42	14	—	6	45
1350-550	125	—	27	12	128
1350-600	160	35	20	14	165
1350-650	159	47	24	11	167
1350-700	153	57	43	14	169

Table 10 Theoretical yield strength reduction and measured yield strength reduction (MPa)

Sample	Solid solution strengthening	Reduced solid solution strengthening	Precipitation strengthening	Theoretical yield strength reduction	Reduced measured yield strength
1350-450	420	—	—	—	—
1350-500	347	73	45	28	78
1350-550	243	178	128	50	80
1350-600	140	280	165	115	108
1350-650	64	356	167	189	165
1350-700	112	309	169	140	416

Obviously, precipitation strengthening was mainly derived from the precipitation phase at 1~5 nm. Kobayashi et al.^[21] also noted that TiC particles of 2~3 nm is the most potent for particle strengthening. Based on the phase analysis results and solid solution strengthening empirical formula in Eq. (2), the solid solution strengthening of samples tempered at different temperatures was calculated after being quenched at 1350 °C. The solid solution strengthening value and measured yield strength of 1350-450 were taken as reference values. The reduction in solid solution strengthening equaled the solid solution strengthening value of 1350-450 minus the other solid solution strengthening values, and the measured yield strength reduction was obtained in the same way. Calculation results are shown in Table 10.

Many researchers^[9, 22, 23.] have used Eq.(5) to describe the yield strength in ferrite steels.

$$\sigma_y = \sigma_0 + \sigma_g + \sigma_s + \sigma_d + \sigma_p \quad (5)$$

where σ_0 is the lattice friction of pure iron, σ_g is the grain refinement strengthening, σ_s is the solid solution strengthening, σ_d is the dislocation strengthening, and σ_p is the precipitation strengthening. In Eq. (5), the dislocation strengthening and precipitation strengthening were added together directly. Yen et al.^[24] calculated the total yield stress using Eq. (6):

$$\sigma_y = \sigma_0 + \sigma_g + \sigma_s + \sqrt{\sigma_d^2 + \sigma_p^2} \quad (6)$$

The dislocation strengthening and precipitation strengthening were not added together directly. According to Li et al.^[25], the original dislocation density was related to the pinning of the precipitated secondary phase particles; the dislocation strengthening could be ignored. Therefore, the author posits that for low-carbon steel, the yield strength equaled the sum of solid strengthening, grain refinement strengthening, and precipitation strengthening. According to Takaki^[26], when calculating ultrafine grain strengthening, the width of the martensitic lath was adopted as the grain size and accompanying with martensite transformation, a large amount of secondary phase particles and dislocation pinned by nanoscale precipitates in steel indicated that ultrafine grain strengthening either included or involved dislocation strengthening and precipitation strengthening. Thus, Takaki stated that the dislocation strengthening, ultrafine grain strengthening, and dislocation strengthening could not be added together. In this research, the dislocation density of 1350-Q, 1350-400, 1350-450, 1350-500, 1350-550, 1350-600, 1350-650, and 1350-700 was 8.9576×10^{11} , 7.9720×10^{11} , 3.5349×10^{11} , 3.1192×10^{11} , 2.8785×10^{11} , 1.8070×10^{11} , 1.2675×10^{11} , and $3.1254 \times 10^{10} \text{ cm}^{-2}$, respectively. Dislocation strengthening can be expressed as follows^[9]:

$$\sigma_d = M\alpha G b \rho^{1/2} \quad (7)$$

where M is the average Taylor factor, α is a constant, G is the shear modulus, b is the Burgers vector, and ρ is the dislocation density. Values were set at $M = 2.75$, $\alpha = 0.435$, $G = 80.3 \text{ GPa}$, and $b = 0.25 \text{ nm}$ as noted in Ref.[9]. Substituting the measured dislocation density of 1350-450 into Eq. (7), the dislocation strengthening amount in 1350-450 was 1427 MPa, higher than the measured yield strength of 1350-450. This result is obviously irrational. Samples quenched at 880 °C and tempered at 450~500 °C indicated that when the tempered martensite lath remained, the reduction in solid solution strengthening was equal to the reduced measured yield strength. The dislocation strengthening can be ignored. In this section tempered martensite lath structures were basically kept within the range of 450~650 °C because the precipitation of nano-sized (Ti,Mo)C particles hindered and delayed the decomposition of tempered martensite lath. As such, dislocation strengthening can be ignored in these conditions. The calculation results presented in Table 10 indicate that a reduction in solid solution strengthening minus precipitation strengthening increment was approximately equal to the small reduction in measured yield strength in the range of 550~650 °C, hence the appearance of the secondary hardening platform.

3 Conclusions

1) In the hot-rolled sample of experimental Cr-Mo steel

with added Ti, some (Ti,Mo)C particles were observed within 18~36 nm, 36~60 nm, and 60~96 nm in size. The (Ti,Mo)C particles had a Ti/Mo ratio of 5~4.

2) When experimental steel was austenitized at 880 °C and tempered at different temperatures, more M_3C were precipitated with an increase in tempering temperature, but no new (Ti,Mo)C particles were precipitated during tempering. Thus, strength and hardness decreased linearly with an increase in tempering temperature.

3) When the experimental steel was austenitized at 1350 °C and tempered at a temperature above 500 °C, some new (Ti,Mo)C particles were precipitated within 1~5 nm. With an increase in the tempering temperature, the precipitation amount grew gradually, and the atomic ratio of Ti/Mo in (Ti,Mo)C particles fell to approximately 1. The (Ti,Mo)C particles precipitated during tempering at a size of 1~5 nm could result in precipitation strengthening with an increment of approximately 165 MPa in yield strength, demonstrating a strong secondary hardening effect.

References

- 1 Xu L, Shi J, Cao W Q *et al. Mater Sci*[J], 2011, 46: 6384
- 2 Weng Y Q, Dong H, Gan Y Eds. *Advanced Steels*[M]. Beijing: Metallurgical Industry Press, 2011 (in Chinese)
- 3 Funakawa Y, Shiozaki T, Tomita K *et al. ISIJ Inter*[J], 2004, 44: 1945
- 4 Yen H W, Chen P Y, Huang C Y *et al. Acta Mater*[J], 2011, 59: 6264
- 5 Wang X P, Zhao A M, Zhao Z Z *et al. Univ Sci & Technol Beijing*[J], 2014, 36: 1183
- 6 Kim Y W, Hong S G, Huh Y H *et al. Mater Sci & Eng A*[J], 2014, 615: 255
- 7 Sun C F, Cai Q W, Wu H B *et al. Acta Metallurgica Sinica*[J], 2012, 48: 1415 (in Chinese)
- 8 Lee S M, Lee J Y. *Acta Metal*[J], 1987, 35: 2695
- 9 Peng Z W, Li L J, Gao J X *et al. Mater Sci & Eng A*[J], 2016, 657: 413
- 10 Wang C J, Sun X J, Yong Q L *et al. Acta Metallurgica Sinica*[J], 2013, 49: 399 (in Chinese)
- 11 Wei F G, Hara T, Tsuchida T *et al. ISIJ Inter*[J], 2003, 43: 539
- 12 Fawakhry K E, Mishreky M L, Eissa M. *Scandinavian Journal of Metallurgy*[J], 1990, 19: 33
- 13 Hu B H, Cai Q W, Wu H B. *J Iron & Steel Res International*[J], 2014, 21: 878
- 14 Cheng L, Cai Q W, Xie B S *et al. Mater Sci & Eng A*[J], 2016, 651: 185
- 15 Jang J, Lee C H, Heo Y *et al. Acta Mater*[J], 2012, 60: 208
- 16 Wang Z Q, Sun X J, Yang Z G *et al. Mater Sci & Eng A*[J], 2013, 573: 84
- 17 Nagao A, Martin M, Dadfarnia M *et al. Acta Mater*[J], 2014, 74: 244
- 18 Lee W Y, Su T T. *J. Mater Process Technol*[J], 1999, 87: 198

- 19 Yong Q L. *Secondary Phase in Steels*[M]. Beijing: Metallurgical Industry Press, 2006 (in Chinese)
- 20 Cheng X Y, Zhang X, Li H et al. *Mater Sci & Eng A*[J], 2015, 636: 164
- 21 Kobayashi Y, Takahashi J, Kawakami K. *Scripta Mater*[J], 2012, 67: 854
- 22 Kim Y W, Kim J Y, Hong S G et al. *Mater Sci & Eng A*[J], 2014, 605: 244
- 23 Kim Y W, Song S W, Seo S J et al. *Mater Sci & Eng A*[J], 2013, 565: 430
- 24 Yen H W, Chen P Y, Huang C Y et al. *Acta Mater*[J], 2011, 59: 6264
- 25 Li X L, Lei C S, Deng X T et al. *J Alloy & Compd*[J], 2016, 689: 524
- 26 Takaki S. *Ferrum*[J], 2008, 13: 304

马氏体钢中(Ti,Mo)C粒子的析出行为和强化效应

靳晓坤^{1,2}, 徐乐¹, 尉文超¹, 姚可夫², 时捷¹, 王毛球¹

(1. 钢铁研究总院, 北京 100081)

(2. 清华大学, 北京 100084)

摘要:为了研究复合(Ti,Mo)C粒子的析出行为和强化效应,选取了一种含钛的Cr-Mo钢作为研究对象,对此钢分别进行880和1350℃淬火并回火。化学萃取相分析结果表明,当淬火温度为880℃时,(Ti,Mo)C粒子的尺寸主要分布在18~36, 36~60, 60~96 nm,这些粒子是在热轧过程中析出的。当淬火温度为1350℃时,回火过程中新析出了1~5 nm的(Ti,Mo)C粒子,这些新析出的(Ti,Mo)C粒子产生了一个明显的二次硬化平台,析出强化量约为165 MPa。新析出的(Ti, Mo)C粒子中的Ti/Mo原子比随回火温度的升高而降低并稳定在1左右。

关键词: 马氏体钢; 回火; (Ti, Mo)C; 强化

作者简介: 靳晓坤, 男, 1987年生, 博士生, 钢铁研究总院特钢所, 北京 100081, E-mail: 2545835925@qq.com